Low-energy dipole γ-ray transition rates in even-even deformed nuclei

V. G. Soloviev, A. V. Sushkov, and N. Yu. Shirikova
Bogoliubov Laboratory of Theoretical Physics, Joint Institute for Nuclear Research, 141980 Dubna, Moscow region, Russia
(Received 22 May 1997)

A study of low-lying magnetic and electric dipole excitations is carried out in ^{166,168}Er, ^{172,174}Yb, and ^{178}Hf within the quasiparticle-phonon nuclear model with the wave functions consisting of one- and two-phonon terms. It is shown that computed $M1$ strength below 4 MeV in these nuclei is much stronger fragmented than in Gd and Dy isotopes in agreement with the relevant experimental observation. The scissors state is strongly fragmented and the overlapping between the scissors state and any 1^+ state is less than 0.1. The fragmentation of the one-phonon 1^+ states, as a rule, is stronger than the fragmentation of the one-phonon states with $K^\pi=0^-$ and 1^-. The resulting $M1$ and $E1$ spectra are compared with available experimental data. The calculated $M1$ and $E1$ strengths summed in the energy range 2–4 MeV are in agreement with the relevant experimental data. [S0556-2813(97)05810-X]

PACS number(s): 21.60.Ev, 21.60.Jz, 27.70.+q

I. INTRODUCTION

A large body of experimental data is now available on magnetic dipole excitations in even-even deformed nuclei [1,2], known as scissors mode [3]. Strong $M1$ transition rates were first discovered in inelastic electron scattering experiments on ^{156}Gd [4] and were found since then in most deformed nuclei. Comparative (e,e') and (p,p') experimental studies have established the orbital character of the mode [5–7]. The measurement of the linear polarization of the scattered protons in nuclear resonance fluorescence experiments has enabled parity assignment [8]. The strong $E1$ transitions in the same energy range of the scissors mode, or immediately below, have been observed [8,9].

The properties of the low-lying $K^\pi=1^+$ states and $M1$ transition rates have been studied in the random-phase approximation (RPA) [10–15]. The energies and wave functions of the $K^\pi=0^-$ and 1^- low-lying states in deformed nuclei are described as one-phonon octupole states. The octupole-octupole interaction is responsible for the strong increase in the $E1$ strength in the excitation energy region 0–4 MeV. It has been shown [16] that additional inclusion of the isovector dipole-dipole interaction decreases the $E1$ strength by more than an order of magnitude, thus bringing it close to experimental data.

Most of the microscopic calculations of the $M1$ and $E1$ transition rates carried out so far have been formulated in a space spanned by two-quasiparticle states. Many two-phonon excitations, however, fall within the energy range where the low-lying $M1$ and $E1$ transitions are observed. In order to study the effect of these states, it is necessary to enlarge the space. This is achieved by using the quasiparticle-phonon nuclear model (QPNM) [17,18].

The low-lying $M1$ transitions have recently been studied within the QPNM in ^{156,158,160}Gd and ^{160,162,164}Dy in Refs. [19, 20]. The $E1$ transitions to the levels below 2.3 MeV were described in [21,22]. The $M1$ and $E1$ transition rates from the ground to excited states below 2.5 MeV in ^{238}U were calculated in [23]. The correlation between $E1$ and $E3$ transition strength was studied in [24].

The aim of this paper is to describe the results of calculation of the $M1$ and $E1$ strength distribution in ^{166,168}Er, ^{172,174}Yb, and ^{178}Hf. This paper is organized as follows. In Sec. II we briefly describe the QPNM. The calculated details and numerical results are given in Sec. III and Sec. IV. A systematics of the results of calculations within the QPNM and comparison with the relevant experimental data and discussion are presented in Sec. V.

II. QUASIPARTICLE-PHONON NUCLEAR MODEL

The initial QPNM Hamiltonian contains the average field of a neutron and a proton system in the form of the axial-symmetric Woods-Saxon potential, monopole pairing, isoscalar and isovector particle-hole (ph), as well as particle-particle (pp) multipole, spin-multipole and tensor interactions between quasiparticles. The effective interactions between quasiparticles are expressed as a series of multipoles and spin-multipoles. It is essential that the interaction between quasiparticles is presented in a separable form. In this paper, we used only the multipole and spin-spin interactions.

We now transform the initial QPNM Hamiltonian. For this purpose we perform a canonical Bogolubov transformation

$$a_{q\sigma}=u_q\alpha_{q\sigma}+\sigma v_q\alpha^+_{q-\sigma} \tag{1}$$

in order to replace the particle operators $a_{q\sigma}$ and $a^+_{q\sigma}$ by the quasiparticle operators $\alpha_{q\sigma}$ and $\alpha^+_{q\sigma}$. We introduce the phonon operators of two types. If we take into account only interactions of the electric type, the phonon creation operator has the following standard form:

$$Q^+_{\lambda\mu i_1\sigma}=\frac{1}{2}\sum_{qq'}\{\psi^{\lambda\mu i_1}_{qq'}A^+(qq';\mu\sigma)-\phi^{\lambda\mu i_1}_{qq'}A(qq';\mu-\sigma)\}. \tag{2}$$

If we take into account electric and magnetic interactions, we write the phonon operator [18] in the form

$$Q^{+}_{\lambda\mu i_1\sigma}=\frac{1}{2\sqrt{2}}\sum_{qq'}\{\psi^{\lambda\mu i_1}_{qq'}(1+i\sigma)A^{+}(qq';\mu\sigma) - \phi^{\lambda\mu i_1}_{qq'}(1-i\sigma)A(qq';\mu-\sigma)\}. \quad (3)$$

The coefficients of the electric part are real; and of the magnetic part, imaginary. Here $i_1=1,2,3\ldots$ is the root number of the RPA secular equation; $A^{+}(qq';\mu\sigma)$ and $A(qq';\mu\sigma)$ are, respectively, pair of creation and annihilation quasiparticle operators. The quantum numbers of the single-particle states are denoted by $q\sigma$, where $\sigma=\pm1$; q equals K^{π} and asymptotic quantum numbers $Nn_z\Lambda\uparrow$ at $K=\Lambda+1/2$ and $Nn_z\Lambda\downarrow$ at $K=\Lambda-1/2$. The RPA one-phonon state is described by the wave function

$$Q^{+}_{\lambda\mu i\sigma}\Psi_0, \quad (4)$$

where Ψ_0 is the ground state wave function of a doubly even nucleus which is determined as a phonon vacuum. The normalization condition of the wave function (4) has the form

$$\frac{1+\delta_{\mu0}}{2}\sum_{qq'}[(\psi^{\lambda\mu i_1}_{qq'})^2-(\phi^{\lambda\mu i_1}_{qq'})^2]=1. \quad (5)$$

After some transformation, the QPNM Hamiltonian becomes

$$H_{\mathrm{QPNM}}=\sum_{q\sigma}\epsilon_q\alpha^{+}_{q\sigma}\alpha_{q\sigma}+H_v+H_{vq}, \quad (6)$$

where the first two terms describe quasiparticles and phonons, and H_{vq} describes the quasiparticle-phonon interaction.

The one-phonon states form the basis of the QPNM. We, therefore, pay much attention to the solution of the RPA equations. At the next stage, the interaction of quasiparticles with phonons is taken into account. The wave function of the excited state is represented as a series with respect to the number of phonon operators. The approximation consists in the truncation of this series.

The one-phonon states with $K^{\pi}=0^{+}$ [denoted by $(\lambda\mu)_i=(20)_i$] are calculated in the RPA with monopole and quadrupole pairing and monopole and ph and pp isoscalar and isovector quadrupole interactions. The relevant RPA equation is given in [18,25]. The one-phonon states with $K^{\pi}=1^{+}$ [denoted by $(21)_i$] are calculated with ph and pp isoscalar and isovector quadrupole and spin-spin interactions. The RPA equations for the $K^{\pi}=1^{+}$ one-phonon states are given in [19,20]. The one-phonon states with $K^{\pi}=0^{-}$ and 1^{-} are calculated in the RPA with the ph and pp isoscalar and isovector octupole and ph isovector dipole interactions. The relevant RPA equations are given in [21,25]. Other phonons ($\lambda\mu=22$, 32, 33, 43, 44, 54, 55, etc.) are calculated with the ph and pp isoscalar and multipole isovector interactions.

To describe nonrotational states in the QPNM, we used a wave function consisting of a sum of one- and two-phonon terms

$$\Psi_n(K^{\pi_0}_0\sigma_0)=\left\{\sum_{i_0}R^n_{i_0}Q^{+}_{g_0}+\sum_{\substack{g_1g_2\\ \sigma_1\sigma_2}}\frac{(1+\delta_{g_1g_2})^{1/2}}{2[1+\delta_{\mu_00}(1-\delta_{\mu_10})]^{1/2}} \times\delta_{\sigma_1\mu_1+\sigma_2\mu_2,\sigma_0\mu_0}P^n_{g_1g_2}Q^{+}_{g_1\sigma_1}Q^{+}_{g_2\sigma_2}\right\}\Psi_0. \quad (7)$$

Here $g_0=\lambda_0\mu_0i_0$, $\mu_0=K_0$, $n=1,2,3\ldots$ is the number of the K^{π} state.

III. CALCULATION DETAILS

A. Numerical procedure

The calculations are made with the Woods-Saxon potential with quadrupole β_2 and hexadecapole β_4 and $\gamma=0$ equilibrium deformations. The single-particle spectrum is taken from the bottom of the potential well up to $+5$ or $+15$ MeV. The parameters of the Woods-Saxon potential were fixed in 1968. $M1$ and $E1$ transition rates from the ground excited up to 4 MeV states were calculated with the wave functions (7).

The isoscalar constants $\kappa^{\lambda\mu}_0$ of ph interactions are fixed so as to reproduce experimental energies of the first $K^{\pi}_{n=1}$ nonrotational states. The calculations were made with the isovector constant $\kappa^{\lambda\mu}_1=-1.5\kappa^{\lambda\mu}_0$ for ph interactions and the constant $G^{\lambda\mu}=0.8\kappa^{\lambda\mu}_0$ for pp interactions. The monopole pairing constants were fixed by pairing energies at $G^{20}=0.8\kappa^{20}_0$. The radial dependence of the multipole interactions has the form $dV(r)/dr$, where $V(r)$ is the central part of the Woods-Saxon potential. The phonon basis consists of ten ($i_0=1,2,\ldots,10$) phonons of each multipolarity: $\lambda\mu=20$, 22, 32, 33, 43, 44, 54, 55, and 65. We used twenty phonons with $\lambda\mu=21,30,31$. The energies of the two-quasiparticle poles were calculated by taking into account the blocking effect and the Gallagher-Moszkowski correction [26]. After the construction of the phonon basis, no free parameters were therefore left. The calculations of nonrotational states in even-even and odd-mass nuclei were performed with the same basis.

B. 1^{+} states

The one-phonon states with $K^{\pi}=1^{+}$ are calculated in the RPA with isoscalar κ^{21}_0 and isovector κ^{21}_1 ph and pp G^{21} quadrupole-quadrupole and isoscalar κ^{011}_0 and isovector κ^{011}_1 spin-spin interactions. In both RPA and QPNM the $M1$ strengths were computed by using a bare orbital gyromagnetic factor and an effective spin factor $g^{\mathrm{eff}}_s=0.7g^{\mathrm{free}}_s$.

The spurious state is approximately excluded by choosing the constant $\kappa^{21}_0>(\kappa^{21}_0)_{\mathrm{cr}}$. The first root of the RPA secular equation equals zero at $(\kappa^{21}_0)_{\mathrm{cr}}$. The overlap between the one-phonon $Q^{+}_{21i}>$ and the spurious $<j_-$ states is given by

$$N^i_{\mathrm{sp}}=\frac{1}{\langle j_-j_+\rangle}\langle j_-Q^{+}_{21i}\rangle\langle Q_{21i}j_+\rangle. \quad (8)$$

TABLE I. Summed overlaps with the spurious and scissors states and $M1$ and $E2$ strengths calculated for different constants κ_0^{21} in the energy range 2–4 MeV in ^{166}Er and ^{178}Hf and in 1–3 MeV in ^{238}U.

Nucleus	κ_0^{21} fm^2 MeV^{-1}	$\Sigma_i N_{\rm sp}^i$	$\Sigma_i Sc^i$	$\Sigma_i B(M1)^i\uparrow$ μ_N^2	$\Sigma_i B(E2)^i\uparrow$ s.p.u.
^{166}Er	0.0143	0.032	0.41	5.11	2.27
	0.0154	0.017	0.42	5.13	1.91
	0.0164	0.012	0.43	5.23	1.68
^{178}Hf	0.0133	0.045	0.31	4.05	2.67
	0.0152	0.013	0.32	3.94	1.98
	0.0164	0.016	0.34	4.04	2.02
^{238}U	0.0130	0.018	0.49	7.10	1.71
	0.0154	0.028	0.52	7.02	1.43
	0.0170	0.063	0.55	6.98	1.41

The sum $\Sigma_i N_{\rm sp}^i$ over the first four states in ^{164}Dy is equal to 0.48 at $\kappa_0^{21}=0.010$ fm^2 MeV^{-1} and to 0.008 at $(\kappa_0^{21})_{\rm cr}=0.01435$ fm^2 MeV^{-1}. The sums $\Sigma_i N_{\rm sp}^i$ over the first twenty states up to 4 MeV and over all levels up to 30 MeV in ^{164}Dy are equal to 0.023 and 0.048, respectively. The total overlap $\Sigma_i N_{\rm sp}^i$ for all levels below 30 MeV in ^{168}Er and ^{238}U is $\Sigma_i N_{\rm sp}^i=0.046$ and 0.11, respectively. For any state with $K^\pi=1^+$ the $N_{\rm sp}^i$ value is smaller than 0.005.

We state that it is not necessary to exclude the spurious state rigorously if a nuclear many-body problem is solved approximately. We performed calculations in the RPA to study the influence of different spurious admixtures on the $M1$ transition rates in ^{166}Er, ^{178}Hf, and ^{238}U. The results of calculations are given in Table I. The first root of the RPA secular equation in ^{238}U equals zero at $(\kappa_0^{21})_{\rm cr}=0.0130$ fm^2 MeV^{-1}. The summed $B(M1)\uparrow$ values of the first twenty states equal $7.0\pm0.1\mu_N^2$ for $\kappa_0^{21}=0.0130$, 0.0134, 0.0154, 0.0160, and 0.0170 fm^2 MeV^{-1}. The increase in the summed overlap from 0.018 to 0.063 and in the largest overlap of the single 1^+ state from 0.005 to 0.016 weakly affects the $M1$ strength. The summed overlap $\Sigma_i N_{\rm sp}^i$ in ^{166}Er and ^{178}Hf decreases with increasing constant κ_0^{21} and strongly increases at $\kappa_0^{21}>0.018$ fm^2 MeV^{-1}. An approximate exclusion of the spurious state is reasonably good.

The constant κ_0^{21} was fixed differently comparing with other constants $\kappa_0^{\lambda\mu}$. We used the constant κ_0^{21} a little larger than $(\kappa_0^{21})_{\rm cr}$ for a better description of the first $K_n^\pi=1_1^+$ state. As is shown in Table I, the summed $B(M1)\uparrow$ values weakly depend on κ_0^{21}. The constant $(\kappa_0^{21})_{\rm cr}$ equals 0.013 -0.015 fm^2 MeV^{-1} in ^{156,158,160}Gd, ^{160,162,164}Dy, ^{166,168}Er, ^{178}Hf, ^{238}U, and ^{240}Pu. The present calculations are performed with the constant κ_0^{21} equal to 0.015 fm^2 MeV^{-1}.

We used the constant $G^{\lambda\mu}$ of pp interactions equal to $0.8\kappa_0^{\lambda\mu}$ for all $\lambda\mu$ including $\lambda\mu=21$. As is shown in [27] and in the present calculations, the summed $\Sigma B(M1)\uparrow$ in the energy range 1–4 MeV increased by a factor of 1.2–1.4 at $G^{21}=\kappa_0^{21}$ compared with $G^{21}=0.8\kappa_0^{21}$. This sum decreased by a factor of 0.8–0.9 at $G^{21}=0$ compared with $G^{21}=0.8\kappa_0^{21}$. The summed $\Sigma B(M1)\uparrow$ weakly depends on κ_1^{21}. This sum does not practically change at $\kappa_1^{21}=-\kappa_0^{21}$ compared with $\kappa_1^{21}=-1.5\kappa_0^{21}$; it increases by a factor of 1.5 at $\kappa_1^{21}=0$. We used $\kappa_1^{21}=-1.5\kappa_0^{21}$ in the rare-earth and $\kappa_1^{21}=-1.2\kappa_0^{21}$ in the actinide regions. A critical analysis of the choice of the constant κ_1^{21} in [28] leads to values which are reasonably close to our value. We correctly described giant isoscalar and isovector quadrupole resonance with these constants.

We used the isoscalar κ_0^{011} and isovector κ_1^{011} constants of the ph spin-spin interaction equal to -0.0024 and -0.024 fm^2 MeV^{-1}. The $M1$ strength in the low energy region depends weakly on κ_1^{011} and κ_0^{011}. The summed $\Sigma B(M1)\uparrow$ up to 3 MeV in ^{240}Pu increases by a factor of 1.24 at $\kappa_1^{011}=-0.0024$ and decreases by a factor of 1.24 at $\kappa_1^{011}=-0.24$ compared with $\kappa_1^{011}=-0.024$ fm^2 MeV^{-1}. The summed spin $M1$ strength in the range 1–15 MeV in ^{154}Sm increases by a factor of 1.25 at $\kappa_1^{011}=-0.012$ compared with $\kappa_1^{011}=-0.048$ fm^2 MeV^{-1}. The calculated spin $M1$ strength in ^{154}Sm summed up to 12 MeV at $\kappa_1^{011}=-0.024$ fm^2 MeV^{-1}, equal to 11.5 μ_N^2, is close to the calculated value of 11.4 μ_N^2 in [29]. The calculated spin $M1$ strength in ^{154}Sm summed in the energy range 5–10 MeV at $\kappa_1^{011}=-0.024$ fm^2 MeV^{-1}, equal to 9.5 μ_N^2, does not contradict the experimental $M1$ strength $\Sigma B_\sigma(M1)=11\pm2\mu_N^2$ [30].

C. $K^\pi=0^-$ and 1^- states

The origin of $E1$ strength in the low-energy region in deformed nuclei has been investigated in [31]. It is known that there are no one-phonon 1^- states below the particle threshold in spherical nuclei. Quadrupole deformation is responsible for the splitting of subshells of a spherical basis into twice-degenerate single-particle states. Due to this splitting, part of the $E1$ strength is shifted to low-lying states. An octupole isoscalar interaction between quasiparticles leads to the formation of collective octupole states. Due to the octupole interaction, the summed $E1$ strength for the transition to $K^\pi=0^-$ and 1^- states in the (0–4) MeV energy region increases by two orders of magnitude. An isovector dipole ph interaction shifts the largest part of $E1$ strength from the low-lying states to the region of the isovector GDR.

The one-phonon states with $K^\pi=0^-$ and 1^- are calculated in the RPA with ph and pp isoscalar and isovector octupole and ph isovector dipole interactions. The isovector constant of the ph dipole interaction is $\kappa_1^{1\mu}=-1.5\kappa_0^{3\mu}$ for the rare-earth and $\kappa_1^{1\mu}=-1.2\kappa_0^{3\mu}$ for the actinide nuclei. The GDR was correctly described with these constants $\kappa_1^{1\mu}$.

It has been shown [16,21] that inclusion of the isovector ph electric dipole interaction decreases the $E1$ strength in the low-energy region by more than an order of magnitude. Nevertheless, the calculated $B(E1)$ values for the excitation of the $K^\pi=0^-$ states are 3–10 times as large as experimental ones. Therefore, we have used the following renormalized effective charge

$$e_{\rm eff}^{(1)}=-\frac{e}{2}\left(\tau_z-\frac{N-Z}{A}\right)(1+\chi). \tag{9}$$

The factor χ is a fitting parameter introduced to quench the too large $E1$ transition probabilities at $\chi=0$. In many papers, for example in [32], a numerical value of $(1+\chi)$ equals 0.3. We calculated the $E1$ reduced transition probabilities in ^{168}Er within the QPNM and fixed $(1+\chi)=\sqrt{0.2}$ by an overall fit of the experimental summed strength in the energy range 1.7–4.0 MeV [33].

IV. NUMERICAL RESULTS

The $K^\pi=1^+$ states below 2 MeV have been observed in one-nucleon transfer reactions and in β decays in a number of even-even deformed nuclei. Most of the properties of the collective scissors mode have been established in (e,e') and (γ,γ') experiments. Microscopic calculations of the $K^\pi=1^+$ states and $B(M1)\uparrow$ values have been carried out so far in the RPA. We calculated in the RPA and QPNM the energies and wave functions of the $K^\pi=1^+$ states and $B(M1)\uparrow$ values in ^{156,158,160}Gd, ^{160,162,164}Dy, and ^{238}U. These results were published in [19,20,23]. Our results of the RPA calculations of the $M1$ strength distribution do not practically differ compared to the calculations [10,13,29].

The results of calculations of the energies, wave functions and $B(M1)\uparrow$ and $B(E1)\uparrow$ values in ^{166,168}Er, ^{172,174}Yb, and ^{178}Hf are given in the form of tables or figures. The experimental data as well as the results of our calculations are presented in Tables II–IV. The calculated structure is given as a contribution of the one-phonon $(\lambda\mu)_i$ and two-phonon $\{(\lambda_1\mu_1)_{i_1},(\lambda_2\mu_2)_{i_2}\}$ components to the normalization of the wave function (7). Then, we list the largest two-quasineutron $\nu\nu$ and two-quasiproton $\pi\pi$ components of the wave function (4) of the one-phonon state $(\lambda\mu)_i$. The $B(E\lambda)\uparrow\equiv B(E\lambda;0^+0_{\rm g.s.}\rightarrow I^\pi K_n)$ with $I=\lambda$ for $\lambda\geqslant 2$ is given in the single-particle units

$$B(E\lambda)\uparrow_{\rm s.p.}=\frac{2\lambda+1}{4\pi}\left(\frac{3}{\lambda+3}\right)(0.12A^{1/3})^{2\lambda}e^2(10\ {\rm fm})^{2\lambda}. \tag{10}$$

A. Scissors mode

The wave function of the scissors state has been defined [34] as

$$\Psi_{\rm sc}=(\langle j_-j_+\rangle\langle j_-j_+\rangle_\nu\langle j_-j_+\rangle_\pi)^{-1/2}\times[I_+(\nu)\langle j_-j_+\rangle_\pi-I_+(\pi)\langle j_-j_+\rangle_\nu]\Psi_0 \tag{11}$$

with the normalization condition

$$(\Psi_{\rm sc}^*\Psi_{\rm sc})=1.$$

Here

$$I_\pm(\tau)=\sum_{i_0} I_\pm^{21i_0}(\tau)\frac{1\mp i}{\sqrt{2}}(Q^+_{21i_0\pm}-Q_{21i_0\mp}),$$

$$I_\pm^{21i_0}(\tau)=\sum_{q_1>q_2}^{\tau}\langle q_1|j_\pm|q_2\rangle u^{(-)}_{q_1q_2}\psi^{21i_0}_{q_1q_2}.$$

The wave function $\Psi_{\rm sc}$ is orthogonal to the spurious state $j_+\Psi_0$. The overlap is calculated in the RPA so as to enforce the following normalization condition:

$$\sum_i|(\Psi_{\rm sc}^*Q^+_{21i\sigma_0}\Psi_0)|^2=1,$$

where the sum extends to all RPA states. The overlap of the wave function (7) with the scissors state has the following form:

$$Sc^n=\frac{1}{\langle j_-j_+\rangle\langle j_-j_+\rangle_\nu\langle j_-j_+\rangle_\pi}\sum_{i_0i_0'}R^n_{i_0}R^n_{i_0'}\times[\langle j_-j_+\rangle_\pi I_+^{21i_0}(\nu)-\langle j_-j_+\rangle_\nu I_+^{21i_0}(\pi)]\times[\langle j_-j_+\rangle_\pi I_+^{21i_0'}(\nu)-\langle j_-j_+\rangle_\nu I_+^{21i_0'}(\pi)]. \tag{12}$$

According to our calculations, the scissors mode fragments over both the low- and high-energy $M1$ excitations. The overlap of scissors with low-lying states up to 4 MeV is about 50%. The other half goes to the high energy states in the range 20–24 MeV. This is consistent with the schematic predictions of the existence of two scissors modes, one at low and the other at high energies [35]. The scissors state is strongly fragmented in the low energy region. According to [11] and our calculations, for any 1^+_n state the Sc^n value is smaller than 0.2. The results on the overlap with the scissors state are similar in RPA and QPNM.

The reduced probability for $M1$ transition from the ground state $0^+_{\rm g.s.}$ to the $1^+_{\rm sc}$ scissors state is

$$B_{\rm sc}(M1;0^+_{\rm g.s.}\rightarrow 1^+_{\rm sc})=2\mu_N^2|(\Psi_{\rm sc}^*\Gamma(M1)\Psi_0)|^2=2\mu_N^2\left|\sum_i\mathcal{A}(M1;0^+_{\rm g.s.}\rightarrow 1^+_i)\right|^2, \tag{13}$$

where $\Gamma(M1)$ is the magnetic dipole operator, $\mathcal{A}(M1;0^+_{\rm g.s.}\rightarrow 1^+_i)$ is the amplitude for $M1$ transition to a relevant one phonon component i of the wave function (11). The sum over i extends to all RPA states. A contribution of the scissors components of the one-phonon state i to the $B(M1)_i$ value equals $10^{-5}-10^{-1}$. The ratio

$$\frac{\Sigma_i B_{\rm sc}(M1\uparrow)_i}{\Sigma_i B(M1\uparrow)_i}=0.05$$

for the sum over all the RPA states below 4 MeV for each scissors component $B_{\rm sc}(M1)_i$. According to calculation with Eq. (13), the ratio

TABLE II. Energies, $M1$ and $E2$ strengths and structure of the QPNM $K^{\pi}=1^{+}$ states in ^{168}Er.

	Experiment [33]		Calculation in the QPNM			
n	E_n MeV	$B(M1)\uparrow$ μ_N^2	E_n MeV	$B(M1)\uparrow$ μ_N^2	$B(E2)\uparrow$ s.p.u.	Structure, %
1			2.10	0.05	0.06	$(21)_1$ 82; $(21)_3$ 7 $\{(31)_1,(32)_1\}$ 5 $(21)_1$: $\nu\nu$633↑-642↑ 80 $\nu\nu$624↑-633↑ 13 $\pi\pi$514↑-523↑ 3
2			2.29	0.04	0.02	$(21)_2$ 93 $\{(32)_1,(33)_3\}$ 2 $(21)_2$: $\pi\pi$411↑-411↓ 98
3	2.494	0.162±0.018	2.33	1.05	0.32	$(21)_1$ 12; $(21)_2$ 3 $(21)_3$ 65; $(21)_5$ 5 $\{(31)_1,(32)_1\}$ 6 $\{(33)_2,(54)_1\}$ 5 $(21)_3$: $\nu\nu$624↑-633↑ 62 $\pi\pi$514↑-523↑ 24 $\nu\nu$512↑-521↑ 7 $\nu\nu$633↑-642↑ 3
4	2.643	(0.063±0.013)	2.60	0.02	2×10^{-5}	$(21)_4$ 88 $\{(32)_1,(33)_1\}$ 5 $(21)_4$: $\nu\nu$521↑-521↓ 91 $\nu\nu$512↑-521↑ 6
5	2.676	0.171±0.18	2.66	1.05	0.01	$(21)_3$ 9; $(21)_5$ 81 $\{(31)_1,(32)_1\}$ 3 $(21)_5$: $\pi\pi$514↑-523↑ 44 $\nu\nu$512↑-521↑ 39 $\nu\nu$521↑-521↓ 6
6	2.694	(0.025±0.005)	2.77	0.02	1×10^{-3}	$(21)_6$ 97 $(21)_6$: $\nu\nu$514↓-512↑ 98
7	2.728	(0.262±0.029)	2.85	0.18	0.29	$(21)_7$ 81 $\{(22)_1,(43)_1\}$ 6 $(21)_7$: $\nu\nu$514↓-523↓ 33 $\nu\nu$512↑-521↑ 33 $\pi\pi$404↓-413↓ 10 $\pi\pi$523↑-532↑ 7 $\pi\pi$514↑-523↑ 5
9	2.792	0.179±0.019	3.05	0.24	0.01	$(21)_{10}$ 68 $\{(31)_1,(32)_1\}$ 14 $\{(33)_2,(54)_1\}$ 4
10	2.798	0.208±0.021	3.11	0.12	0.08	$(21)_7$ 4; $(21)_9$ 65 $(21)_{12}$ 11 $\{(22)_1,(43)_1\}$ 9
11	3.048	(0.105±0.014)	3.16	0.58	1×10^{-3}	$(21)_7$ 6; $(21)_9$ 33 $(21)_{12}$ 25; $(21)_{13}$ 6 $\{(22)_1,(43)_1\}$ 14 $\{(32)_1,(33)_1\}$ 5 $\{(33)_2,(54)_1\}$ 5
12	3.357	(0.348±0.041)	3.22	0.11	3×10^{-3}	$(21)_{10}$ 11; $(21)_{12}$ 3 $(21)_{13}$ 4; $(21)_{14}$ 4 $\{(33)_2,(54)_1\}$ 51 $\{(31)_1,(32)_1\}$ 13 $\{(22)_1,(43)_1\}$ 8
13	3.390	0.753±0.086	3.29	0.22	l0.03	$(21)_4$ 3; $(21)_5$ 3 $(21)_{13}$ 4; $(21)_{14}$ 7 $\{(32)_1,(33)_1\}$ 69 $\{(33)_2,(54)_1\}$ 3 $\{(22)_1,(43)_1\}$ 3 $\{(21)_1,(22)_1\}$ 2

TABLE II. (*Continued*).

	Experiment [33]		Calculation in the QPNM			
n	E_n MeV	$B(M1)\uparrow$ μ_N^2	E_n MeV	$B(M1)\uparrow$ μ_N^2	$B(E2)\uparrow$ s.p.u.	Structure, %
14	3.409	(0.234 ± 0.029)	3.34	0.08	1×10^{-4}	$(21)_{12}$ 10; $(21)_{13}$ 18
						$\{(21)_1,(22)_1\}$ 65
						$\{(32)_1,(33)_1\}$ 4
17	3.457	0.319 ± 0.039	3.41	0.02	0.02	$\{(33)_1,(54)_1\}$ 92
18	3.591	(0.055 ± 0.010)	3.44	0.06	0.02	$(21)_3$ 8; $(21)_5$ 4; $(21)_{10}$ 7
						$\{(31)_1,(32)_1\}$ 49
						$\{(33)_2,(54)_1\}$ 15
19	3.657	(0.191 ± 0.026)	3.48	0.13	0.16	$(21)_{12}$ 3; $(21)_{14}$ 27
						$\{(32)_1,(33)_2\}$ 27
						$\{(44)_1,(43)_1\}$ 5
						$\{(22)_1,(33)_1\}$ 10
						$\{(33)_1,(54)_1\}$ 5
26	3.776	(0.054 ± 0.010)	3.74	0.05	4×10^{-5}	$(21)_{12}$ 9; $(21)_{13}$ 8
						$(21)_{14}$ 4
						$\{(22)_1,(43)_1\}$ 31
						$\{(33)_3,(54)_1\}$ 22
42	3.806	0.204 ± 0.033	3.94	0.04	0.01	$(21)_{15}$ 7
						$\{(30)_1,(31)_2\}$ 81

$$\frac{B_{\rm sc}(M1;0^+_{\rm g.s.}\rightarrow1^+_{\rm sc})}{\Sigma_i B(M1\uparrow)_i}=0.3-0.4.$$

It means that the scissors contribution to the total $M1$ strength in the energy range 1–4 MeV is large due to the coherence effect.

The scissors mode is mostly responsible for enhanced total $M1$ strength in the low-energy region. The contribution of the scissors state to the total $M1$ strength in the energy range up to 30 MeV in ^{168}Er equals 60%. The large contribution to the total $M1$ strength in the energy range 2–30 MeV is due to the coherence sum in Eq. (13). Nevertheless, its contribution to the wave functions of each 1^+ states is small. The wave functions of $K^\pi=1^+$ states are mostly determined by other components which may be observed, for example, by one-nucleon-transfer reactions.

B. $K^\pi=1^+$ states and $M1$ strength distribution

The fragmentation of the one-phonon $K^\pi=1^+$ states in ^{156,158,160}Gd and ^{160,162,164}Dy has been studied in the QPNM in [19,20]. In each of these nuclei there is a strong peak of an order of $1–1.5\mu_N^2$. The fragmentation is appreciable only above 3 MeV.

In our investigation of the fragmentation of one-phonon states we paid special attention to ^{168}Er because the parities of the excited states have been determined model independently by measuring the linear polarization of the scattered photons. Experimental energies of the 1^+ states and $B(M1)\uparrow$ values [33] are compared with the calculated ones in Table II. The $B(E2)\uparrow$ values characterize the collectivity of each state. The structure of each $K^\pi=1^+$ state is presented. The 1^+ levels below 2.3 MeV in ^{168}Er have not been observed experimentally. It is impossible to compare one to one the experimental and computed levels.

The experimental and computed $M1$ strength distributions in ^{166}Er are given in Fig. 1. In general, the observed $M1$ strength in ^{168}Er and ^{166}Er is stronger fragmented than in the Gd and Dy isotopes. The fragmentation of one-phonon states due to the coupling with two-phonon configurations is very important above 3 MeV in both nuclei. The observed $M1$ strength in ^{166,168}Er is stronger fragmented below 3 MeV than the calculated ones.

The experimental and calculated $M1$ strength distribution in ^{172}Yb is given in Fig. 2. The experimental and calculated energies and $B(M1)\uparrow$ values in ^{174}Yb are presented in Table III. The first $K_n^\pi=1_1^+$ state with energy 1.624 MeV in ^{174}Yb is, practically, pure two-quasineutron state. This state was observed in the (d,p) reaction [36]. This two-quasineutron $\nu\nu514\downarrow-512\uparrow$ state was not observed in ^{172}Yb. The second $K_n^\pi=1_2^+$ 2.01 MeV state in ^{172}Yb was observed in the (d,t) reaction. Most levels with $K^\pi=1^+$ in ^{172}Yb and ^{174}Yb were observed in the (γ,γ') experiments [37] with uncertain parity assignments. The parity of the levels with energy 3.349 and 3.562 MeV in ^{174}Yb are known from the (e,e') experiments [38]. According to our calculation, the two-quasiproton state $\pi\pi404\downarrow-413\downarrow$ is fragmented in the energy range 3.5–3.9 MeV in ^{174}Yb. Therefore, this configuration has not been observed in the (t,α) reaction [39].

A comparison of the observed $M1$ strength distribution in ^{178}Hf [40] with the result of the present calculations within the RPA and QPNM is demonstrated in Fig. 3. The strong fragmentation of the $M1$ strength in the energy range 2.4–4.0 MeV is well described in the QPNM. According to the RPA calculation, there is a strong peak of $1.05\mu_N^2$ at 3.64

TABLE III. Energies, $M1$ and $E2$ strengths and structure of the QPNM $K^{\pi}=1^{+}$ states in ^{174}Yb.

	Experiment [37]		Calculation in the QPNM			
n	E_n MeV	$B(M1)\uparrow$ μ_N^2	E_n MeV	$B(M1)\uparrow$ μ_N^2	$B(E2)\uparrow$ s.p.u.	Structure, %
1	1.624		1.60	1.3×10^{-3}	3×10^{-4}	$(21)_1$ 99
						$(21)_1$: $\nu\nu$514↓-512↑ 99
2	2.037	0.15±0.11	2.10	0.86	0.87	$(21)_2$ 99
	2.068	0.20±0.12				$(21)_2$: $\nu\nu$624↑-633↑ 72
						$\pi\pi$514↑-523↑ 13
3	2.338	0.28±0.10	2.65	0.92	0.02	$(21)_3$ 85; $(21)_5$ 1
	2.500	0.35±0.11				$(21)_6$ 2
						$\{(22)_1,(43)_1\}$ 2
						$\{(31)_2,(32)_1\}$ 3
						$\{(32)_1,(33)_1\}$ 1
						$\{(54)_1,(55)_1\}$ 2
						$(21)_3$: $\pi\pi$514↑-523↑ 45
						$\nu\nu$633↑-642↑ 30
						$\nu\nu$512↑-521↑ 15
						$\nu\nu$514↓-523↓ 5
5	2.581	(0.21±0.08)	2.69	0.11	0.06	$(21)_5$ 55; $(21)_6$ 18
						$(21)_8$ 2
						$\{(32)_1,(33)_1\}$ 12
						$\{(31)_2,(32)_1\}$ 3
						$(21)_5$: $\nu\nu$615↑-624↑ 38
						$\nu\nu$633↑-642↑ 25
						$\pi\pi$514↑-523↑ 16
						$\nu\nu$510↑+521↓ 9
						$\nu\nu$512↑-521↑ 6
11	2.920	(0.44±0.11)	3.06	0.25	0.03	$(21)_8$ 5; $(21)_9$ 8
						$(21)_{10}$ 63; $(21)_{11}$ 6
						$\{(21)_1,(22)_1\}$ 1
						$\{(21)_1,(43)_1\}$ 2
						$\{(31)_1,(32)_1\}$ 9
						$(21)_{10}$: $\nu\nu$512↑-512↓ 66
						$\pi\pi$411↑-411↓ 24
						$\nu\nu$514↓-523↓ 5
14	3.122	(0.10±0.06)	3.21	0.30	0.16	$(21)_{11}$ 28; $(21)_{12}$ 43
	3.145	(0.13±0.06)				$(21)_{13}$ 3; $(21)_{15}$ 5
						$\{(22)_1,(43)_1\}$ 2
						$\{(22)_1,(43)_2\}$ 7
						$\{(31)_2,(32)_1\}$ 3
17	3.349	0.33±0.14	3.35	0.56	0.18	$(21)_{11}$ 4; $(21)_{12}$ 22
						$(21)_{13}$ 13; $(21)_{15}$ 14
						$\{(22)_1,(43)_1\}$ 30
						$\{(32)_1,(33)_1\}$ 3
23	3.562	0.41±0.10	3.57	0.25	0.02	$(21)_{12}$ 4; $(21)_{13}$ 30
						$(21)_{15}$ 13; $(21)_{16}$ 8
						$\{(22)_1,(43)_2\}$ 9
						$\{(22)_1,(43)_3\}$ 3
						$\{(32)_1,(33)_1\}$ 19
						$\{(32)_1,(33)_2\}$ 3
25	3.695	(0.33±0.13)	3.65	0.11	0.03	$(21)_{13}$ 3; $(21)_{15}$ 5
						$\{(21)_2,(20)_1\}$ 66
						$\{(22)_1,(43)_1\}$ 11
						$\{(43)_1,(44)_2\}$ 4
31			3.75	0.22	0.007	$(21)_{15}$ 3; $(21)_{16}$ 3
						$\{(54)_1,(55)_1\}$ 82

TABLE III. (*Continued*).

	Experiment [37]		Calculation in the QPNM			
n	E_n MeV	$B(M1)\uparrow$ μ_N^2	E_n MeV	$B(M1)\uparrow$ μ_N^2	$B(E2)\uparrow$ s.p.u.	Structure, %
33			3.84	0.13	0.11	$(21)_{15}$ 5; $(21)_{16}$ 11 $(21)_{17}$ 4 $\{(21)_2,(22)_1\}$ 41 $\{(22)_1,(43)_2\}$ 10
35			3.87	0.11	0.09	$(21)_{15}$ 5; $(21)_{16}$ 9 $(21)_{17}$ 3 $\{(21)_2,(22)_1\}$ 37 $\{(22)_1,(43)_2\}$ 17 $\{(22)_1,(43)_3\}$ 14

MeV. This one-phonon state is strongly fragmented in the energy range 3.2–4.0 MeV. The coupling between one- and two-phonon states is responsible for strong fragmentation of the $M1$ strength in ^{178}Hf.

C. $K^\pi=0^-$ and 1^- states and $E1$ strength distribution

The rich experimental data on the $E1$ strength distribution in ^{168}Er in the energy range 1.7–4.0 MeV were given in Ref. [33]. We used these data for renormalization of the $E1$ effective charge. The experimental energies and $B(E1)\uparrow$ values and the calculated energies, $B(E1)\uparrow$ and $B(E3)\uparrow$ values and structure of the $K^\pi=0^-$ and 1^- states in ^{168}Er are given in Table IV. The experimental $B(E1)\uparrow$ values in brackets mean that there is somewhat uncertain assignments of parity or/and K-quantum number. The calculated $B(E3)\uparrow$ values for excitation of the $I^\pi K_n=3^-1_1$ and 3^-0_1 states are in agreement with the relevant experimental data. The observed $E1$ strength distribution of the $E1$, $\Delta K=0$ strength below 3.2 MeV is somewhat stronger fragmented than the calculated ones. In general, strong fragmentation of the $E1$ strength in ^{168}Er is reasonably well described in the QPNM. As is shown in Fig. 4, the observed fragmentation of the one-phonon states with $K^\pi=0^-$ in ^{174}Yb is relatively weak. Nevertheless, the observed $E1$, $\Delta K=0$ strength in ^{174}Yb is stronger fragmented than the calculated ones.

A comparison between the observed fragmentation of the $E1$ strength with $\Delta K=0$ and the calculated within the QPNM fragmentation of the $E1$ strengths with $\Delta K=0$ and 1 in ^{166}Er, ^{172}Yb, and ^{178}Hf are presented in Fig. 5, 6, and 7. The observed fragmentation of the $E1$, $\Delta K=0$ strengths are stronger in ^{166}Er and ^{172}Yb and weaker in ^{178}Hf compared to the calculated ones.

V. DISCUSSION

There are quadrupole excitations with $K=0$, 1, and 2 in even-even deformed nuclei. Energies of the first $K_n^\pi=0_1^+$ and 2_1^+ states are lying below the relevant first poles and their wave functions are the superposition of many two-quasiparticle components. Energies of the first $K_n^\pi=1_1^+$ states are lying above the first poles and $B(E2)\uparrow$ values for excitations of the $I^\pi K_n=2^+1_1$ states are very small. The wave functions of each first 1_1^+ state are, practically, two-quasiparticle ones. This difference is connected with approximate excluding of the spurious 1^+ state by choosing the constant $\kappa_0^{21}\geqslant(\kappa_0^{21})_{\rm cr}$. The existing experimental data on the first 1^+ states in deformed nuclei support this method of exclusion of the spurious 1^+ rotational state.

The equilibrium quadrupole deformation is responsible for splitting of subshells of the spherical basis to twice degenerated levels. Due to this splitting, the low-energy collective magnetic dipole excitations exist in deformed nuclei. Therefore, the correlation between $B(M1)\uparrow$ and $B(E2;0^+0_{\rm g.s.}\rightarrow 2^+0_{\rm g.s.})$ takes place [41]. The energies and structure of the $K^\pi=1^+$ states below 4 MeV are mostly determined by the isoscalar ph quadrupole-quadrupole interaction. An admixture of the scissors state to each intrinsic one is very small. The two-quasiparticle structure of the large one-phonon terms of the wave function (7) can be observed in the one-nucleon-transfer reaction. As is shown in [42], the large two-phonon component of the wave function (7) can be detected by fast $M1$ transition rates to the excited state differing by one-phonon with the $K^\pi=1^+$.

The experimental summed $M1$ strengths in the given energy range [43] and the results of the present calculation in several even-even deformed nuclei are given in Table V. As is shown in Table I, the summed in low-energy region $M1$ strengths weakly depend on the constant $\kappa_0^{21}>(\kappa_0^{21})_{\rm cr}$. Therefore, we calculated the summed $M1$ strengths in all nuclei in Table V with the same constants equal to $\kappa_0^{21}=0.015$ fm^2 MeV^{-1} and $G^{21}=0.8\kappa_0^{21}$. There is a very good agreement between the experimental and computed summed $M1$ strengths in all nuclei. The summed $M1$ strength calculated with the same constants κ_0^{21} and G^{21} in ^{238}U in the energy range 2.1–2.5 MeV is equal to $3.3\mu_N^2$ [23], which is in agreement with the experimental values $3.19\mu_N^2$ and $4.0\mu_N^2$ observed respectively in the (γ,γ') and (e,e') reactions [44].

Let us consider a contribution of the orbital and spin parts of the $M1$ transition operator in the $M1$ strength distribution in the energy range 2–14 MeV. The result of the RPA calculation of the total $\Sigma B_{\rm tot}(M1)\uparrow$, orbital $\Sigma B_l(M1)\uparrow$ and spin $\Sigma B_\sigma(M1)\uparrow$ parts, summed in bins of 1 MeV, in ^{154}Sm is presented in Fig. 8. Most of the $M1$ transitions in the energy

TABLE IV. Energies, $E1$ and $E3$ strengths and structure of the QPNM $K^\pi = 0^-$ and 1^- states in ^{168}Er.

	Experiment [33]		Calculation in the QPNM			
K^π_n	E_n MeV	$B(E1)\uparrow$ e^2 fm$^2\times10^{-3}$	E_n MeV	$B(E1)\uparrow$ e^2 fm$^2\times10^{-3}$	$B(E3)\uparrow$ s.p.u.	Structure, %
1^-_1	1.358		1.30	5.90	2.75	$(31)_1$ 95 $\{(22)_1,(33)_2\}$ 3 $(31)_1$: $\nu\nu$633↑-512↑ 81 $\nu\nu$633↑-523↓ 2
0^-_1	1.786	22.38±2.51	1.85	17.3	2.80	$(30)_1$ 99 $(30)_1$: $\nu\nu$512↑-642↑ 30 $\nu\nu$514↓-633↑ 4 $\pi\pi$523↑-404↓ 3
1^-_2	1.937	0.79±0.11	1.92	1.4	0.72	$(31)_2$ 96 $(31)_2$: $\nu\nu$633↑-523↓ 89 $\nu\nu$633↑-512↑ 6
0^-_2	2.137	(1.34±0.25)	2.30	6.9	0.93	$(30)_2$ 99 $(30)_2$: $\nu\nu$514↓-633↑ 19 $\nu\nu$512↑-642↑ 16 $\pi\pi$523↑-404↓ 9
1^-_3	2.342	(0.52±0.11)	2.28	6.0	3.31	$(31)_3$ 94 $(31)_3$: $\nu\nu$651↑-521↓ 31 $\nu\nu$633↑-512↑ 10 $\nu\nu$633↑-523↓ 7 $\nu\nu$642↑-521↑ 5 $\pi\pi$523↑-402↑ 4 $\pi\pi$532↑-411↑ 4
0^-_3	2.417	1.61±0.27	2.49	0.1	9×10^{-3}	$(30)_3$ 99 $(30)_3$: $\pi\pi$523↑-404↓ 32 $\nu\nu$514↓-633↑ 17
0^-	2.510	0.55±0.16				
1^-_4			2.55	4.3	1.79	$(31)_4$ 91 $\{(22)_1,(33)_1\}$ 3 $\{(43)_2,(54)_1\}$ 3 $(31)_4$: $\nu\nu$651↑-521↓ 66 $\nu\nu$642↑-521↑ 3 $\pi\pi$532↑-411↑ 3
0^-_4	2.740	0.80±0.14	2.72	7.0	0.85	$(30)_4$ 88 $\{(22)_1,(32)_1\}$ 4 $\{(44)_1,(54)_1\}$ 3 $(30)_4$: $\nu\nu$523↓-642↑ 28 $\nu\nu$514↓-633↑ 5 $\pi\pi$523↑-404↓ 4
1^-_6	2.849	(1.10±0.15)	2.90	0.1	0.014	$(31)_5$ 95 $\{(22)_1,(33)_3\}$ 3 $(31)_5$: $\pi\pi$523↑-413↓ 92 $\nu\nu$642↑-521↑ 4
0^-_5	2.946	2.06±0.27	3.03	5.3	0.79	$(30)_5$ 86; $(30)_4$ 3 $(30)_6$ 3 $\{(22)_1,(32)_1\}$ 7 $(30)_5$: $\nu\nu$523↓-642↑ 18 $\nu\nu$514↓-633↑ 10
1^-_7	2.975	(0.84±0.15)	3.07	0.1	0.13	$(31)_6$ 37; $(31)_7$ 5 $(31)_8$ 4; $(31)_{10}$ 8 $(31)_{12}$ 6 $\{(20)_3,(31)_1\}$ 27 $\{(22)_1,(31)_1\}$ 5
1^-_8	3.095	(1.04±0.14)	3.09	0.1	6×10^{-3}	$(31)_6$ 34; $(31)_7$ 36

TABLE IV. (*Continued*).

	Experiment [33]		Calculation in the QPNM			
K_n^π	E_n MeV	$B(E1)\uparrow$ e^2 fm$^2\times10^{-3}$	E_n MeV	$B(E1)\uparrow$ e^2 fm$^2\times10^{-3}$	$B(E3)\uparrow$ s.p.u.	Structure, %
						$(31)_8$ 7
						$\{(22)_1,(31)_1\}$ 14
0_6^-	3.181	1.96±0.28	3.19	12.2	1.86	$(30)_6$ 68; $(30)_5$ 8
						$(30)_4$ 5
						$\{(22)_1,(32)_1\}$ 7
						$\{(22)_1,(32)_2\}$ 5
						$\{(44)_1,(54)_1\}$ 5
1_{10}^-	3.190	(1.16±0.15)	3.15	0.4	0.08	$(31)_6$ 17; $(31)_7$ 29
						$(31)_8$ 9; $(31)_{12}$ 10
						$\{(20)_3,(31)_1\}$ 23
						$\{(22)_1,(31)_1\}$ 5
0_8^-	3.441	(0.58±0.15)	3.49	0.3	7×10^{-3}	$(30)_6$ 6; $(30)_8$ 5
						$\{(22)_1,(32)_1\}$ 20
						$\{(22)_2,(32)_1\}$ 45
						$\{(44)_1,(54)_1\}$ 14
						$\{(22)_1,(32)_2\}$ 5
						$\{(43)_1,(33)_2\}$ 2
1_{21}^-	3.468	(1.81±0.26)	3.48	0.2	0.03	$(31)_9$ 4; $(31)_{15}$ 3
						$\{(20)_1,(31)_1\}$ 76
						$\{(43)_1,(54)_2\}$ 6
						$\{(43)_2,(54)_1\}$ 3
0_9^-	3.480	3.64±0.52	3.51	0.4	4×10^{-3}	$(30)_6$ 6; $(30)_8$ 4
						$\{(22)_1,(32)_1\}$ 16
						$\{(22)_2,(32)_1\}$ 54
						$\{(44)_1,(54)_1\}$ 9
0_{13}^-	3.505	(0.53±0.24)	3.67	0.1	4×10^{-6}	$(30)_7$ 6
						$\{(21)_1,(31)_1\}$ 83
1_{22}^-	3.516	(1.31±0.24)	3.49	0.3	0.08	$(31)_{10}$ 7; $(31)_{11}$ 3
						$(31)_{12}$ 9; $(31)_{15}$ 4
						$\{(43)_1,(54)_2\}$ 22
						$\{(20)_3,(31)_1\}$ 20
0_{14}^-	3.703	(1.57±0.31)	3.71	1.5	0.12	$(30)_7$ 37
						$\{(21)_1,(31)_1\}$ 11
						$\{(20)_3,(30)_1\}$ 38
						$\{(43)_1,(33)_3\}$ 6
1_{35}^-	3.719	(1.27±0.32)	3.76	1.0	0.11	$(31)_{15}$ 32
						$\{(20)_1,(31)_3\}$ 17
						$\{(22)_1,(31)_3\}$ 6
						$\{(22)_3,(31)_1\}$ 22

range 2–4 MeV are of the orbital nature. The total $M1$ strength is larger than the sum of the orbital and spin parts. It means that the coherent coupling of the orbital and spin parts takes place in the energy range 2–4 MeV.

There is a destructive interference of the orbital and spin parts of the $M1$ transition operator in the energy range 6–10 MeV. The summed spin $M1$ strength is larger than the total $M1$ strength. The spin $M1$ strength in the energy range 6–7 MeV is by a factor of 1.8 larger than the sum of the orbital and spin parts, calculated separately. The computed total $M1$ strength within 6–7 MeV is larger than the $M1$ strength derived in [45] from the ^{154}Sm (γ,γ') experiment. There is almost no complete cancellation of the $M1$ strength above 6 MeV.

The spin $M1$ strength dominates at energies above 6 MeV. The total $M1$ strength summed up to 30 MeV in ^{168}Er is practically equal to the sum of the orbital and spin $M1$ parts.

There are low-lying collective octupole states with $K^\pi=0^-$ and 1^- in most even-even deformed nuclei. In contrast with strongly dipole exciting $I^\pi 0_n=1^-0_1$ states in many nuclei no indication of these states was found in ^{178}Hf [40]. According to calculation in [46] within the QPNM, the first $K_n^\pi=0_1^-$ state in ^{178}Hf has energy around 2 MeV and

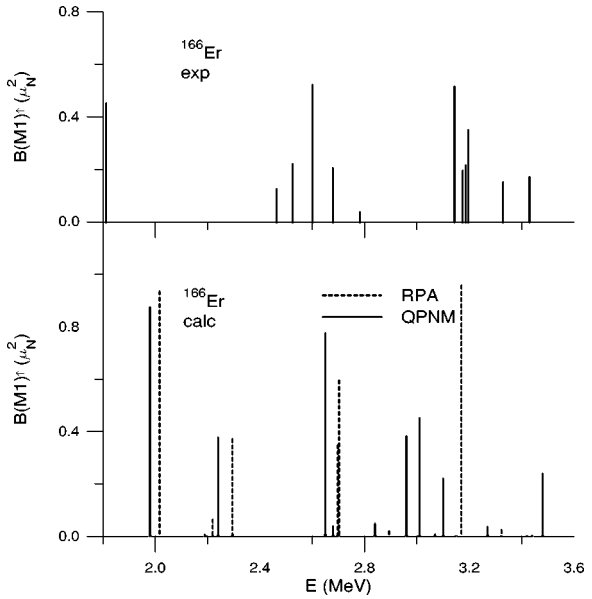

FIG. 1. Experimental, QPNM and RPA $M1$ strength distribution in ^{166}Er. Full and dashed lines refer respectively to QPNM and RPA.

$B(E1;0^+0_{\text{g.s.}} \rightarrow 1^-0_1) = 0.8\times10^{-3}\ e^2\ \text{fm}^2$. The calculated reduced $E1$ transitions to the first $K^\pi_n = 1^-_1$ 1.31 MeV and second 1^-_2 1.513 MeV states are $0.14\times10^{-3}\ e^2\ \text{fm}^2$ and $0.3\times10^{-3}\ e^2\ \text{fm}^2$, respectively.

The existence of strongly dipole excited $K^\pi = 0^-$ states in the energy range 2–4 MeV is a common phenomenon in even-even deformed nuclei. Only a few $E1$ transitions from the ground state to the $K^\pi = 1^-$ states were observed. Therefore, we compare the experimental data with the computed ones for transitions to the $K^\pi = 0^-$ states. The experimental and computed summed $E1$ strengths in the given energy range are given in Table VI. Agreement between experimental and computed data is quite good. The large summed $E1$ strengths in ^{166,168}Er are due to very large $B(E1)$ values for transitions to the first $K^\pi_n = 0^-_1$ states. Strong $E1$ transitions in ^{172}Yb are shifted to higher excitations.

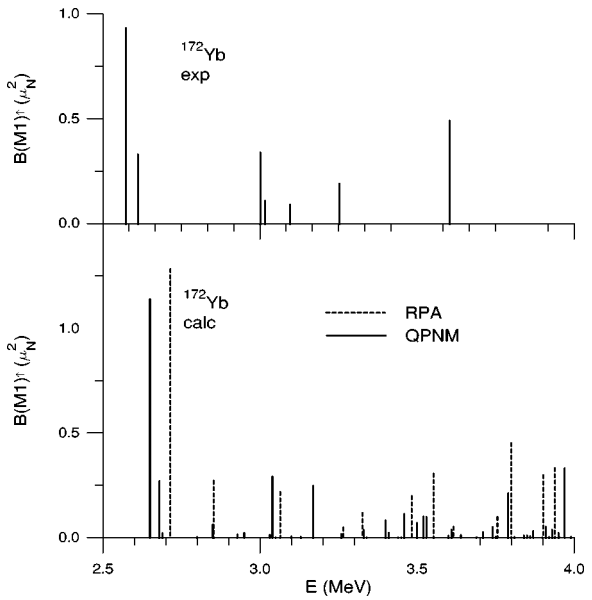

FIG. 2. Experimental, QPNM and RPA $M1$ strength distribution in ^{172}Yb. See Fig. 1 for explanatory details.

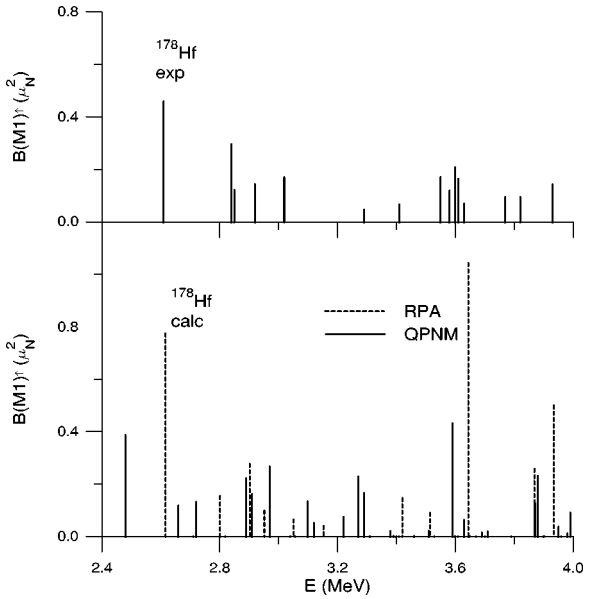

FIG. 3. Experimental, QPNM and RPA $M1$ strength distribution in ^{178}Hf. See Fig. 1 for explanatory details.

According to the experimental data [40], in ^{178}Hf comparably strong excited states are missing and summed $E1$ strength in the energy range 2–4 MeV is decreased compared to deformed nuclei of the rare-earth region. We correctly described this decreasing. The summed $E1$ strength decreases in ^{178}Hf due to the small $E1$ matrix elements between the single-particle states near the Fermi levels in the neutron and proton systems.

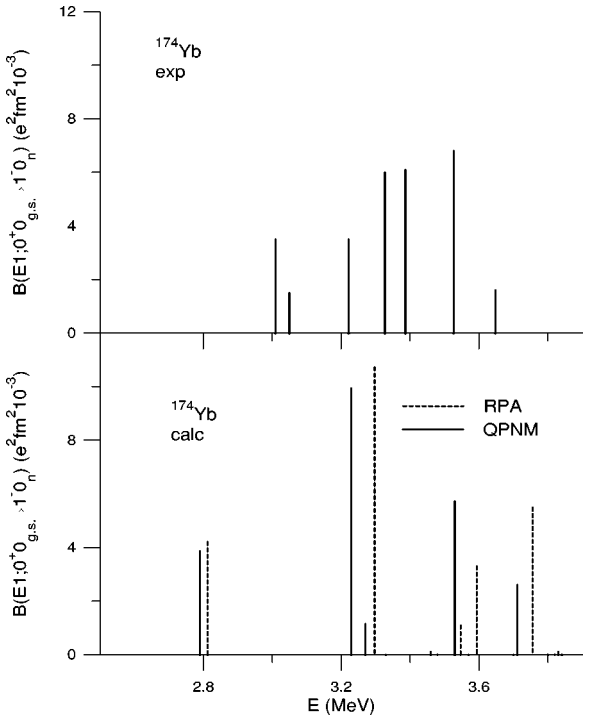

FIG. 4. Experimental, QPNM and RPA $E1$, $\Delta K = 0$ strength distribution in ^{174}Yb. See Fig. 1 for explanatory details.

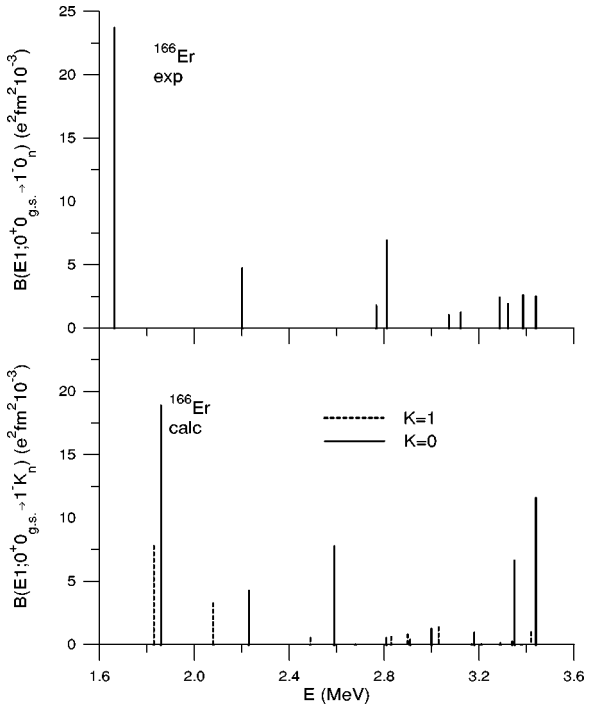

FIG. 5. Experimental $B(E1;0^+0_{\text{g.s.}}\rightarrow 1^-0_n)$ and QPNM $B(E1;0^+0_{\text{g.s.}}\rightarrow 1^-K_n)$ values in ^{166}Er. Full and dashed lines refer respectively to $K=0$ and $K=1$.

According to the QPNM calculations [24], there is a strong correlation between the largest $B(E1)\uparrow$ and $B(E3)\uparrow$ values with excitations of the $I^\pi K=1^-0$, 1^-1, 3^-0, and 3^-1 states. The calculated correlation coefficient r between the $B(E1)\uparrow$ and $B(E3)\uparrow$ values equals 0.987 in ^{160}Gd, ^{160,162,164}Dy [24] and 0.998 in ^{238}U and ^{240}Pu [23] for the

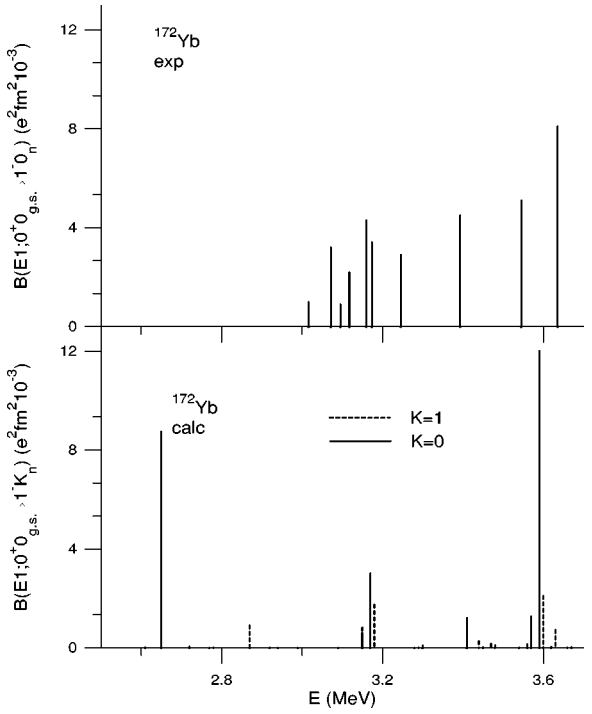

FIG. 6. Experimental $B(E1;0^+0_{\text{g.s.}}\rightarrow 1^-0_n)$ and QPNM $B(E1;0^+0_{\text{g.s.}}\rightarrow 1^-K_n)$ values in ^{172}Yb. See Fig. 5 for explanatory details.

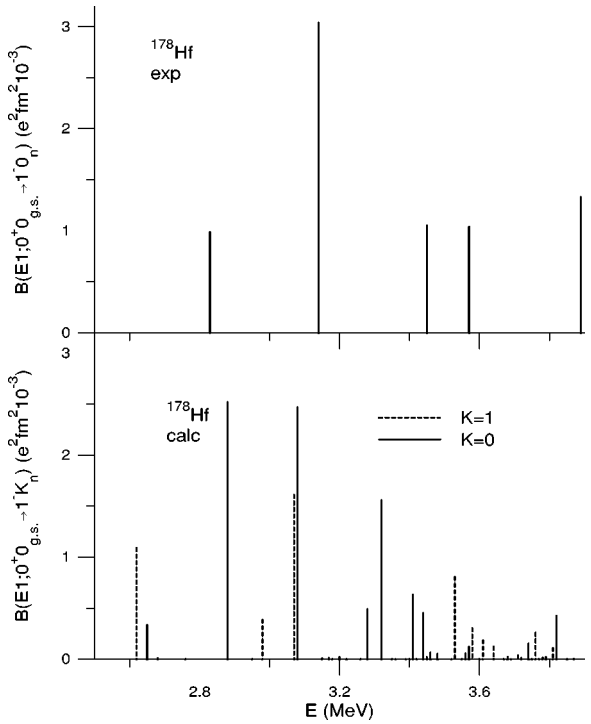

FIG. 7. Experimental $B(E1;0^+0_{\text{g.s.}}\rightarrow 1^-0_n)$ and QPNM $B(E1;0^+0_{\text{g.s.}}\rightarrow 1^-K_n)$ values in ^{178}Hf. See Fig. 5 for explanatory details.

$K^\pi=0^-$ states and 0.910 in ^{160}Gd, ^{160,162,164}Dy and 0.995 in ^{238}U and ^{240}Pu for the $K^\pi=1^-$ states. According to the present calculation, the coefficient r equals 0.96 in ^{166}Er for the $K^\pi=0^-$ and 1^- states and 0.75 for the $K^\pi=0^-$ states and 0.87 for the $K^\pi=1^-$ in ^{172}Yb, ^{174}Yb, and ^{178}Hf. It means that the correlation between $B(E1)\uparrow$ and $B(E3)\uparrow$ values is a general property in even-even deformed nuclei.

Let us consider the intensities of the $M1$ and $E1$ transitions to excited states between 2 MeV and 4 MeV in even-even deformed nuclei. According to the experimental data [33], the $M1$ and $E1$ reduced widths in ^{168}Er summed in the energy range 2–4 MeV are the following:

$$\sum_n \Gamma_0^{\text{red}}(M1;0^+0_{\text{g.s.}}\rightarrow 1^+1_n)=11.6\ \text{meV/MeV}^3,$$

TABLE V. Summed $M1$ strengths in even-even nuclei.

Nucleus	E [MeV]	$\Sigma B(M1)\uparrow[\mu_N^2]$ Expt. [43]	$\Sigma B(M1)\uparrow[\mu_N^2]$ Calc. QPNM
^{156}Gd	2.7–3.7	2.73	2.95
^{158}Gd	2.7–3.7	3.39	3.41
^{160}Gd	2.7–3.7	2.97	2.86
^{160}Dy	2.7–3.7	2.42	2.46
^{162}Dy	2.7–3.7	2.49	2.60
^{164}Dy	2.7–3.7	3.18	2.92
^{166}Er	2.4–3.7	2.67	2.51
^{168}Er	2.4–3.7	2.82	2.87
^{172}Yb	2.4–3.7	1.94	2.25
^{174}Yb	2.4–3.7	2.70	2.84
^{178}Hf	2.4–3.7	2.04	2.30

TABLE VI. Summed $E1$ strengths in even-even deformed nuclei.

Nucleus	E [MeV]	$\Sigma_n B(E1;0^+0_{\text{g.s.}}\rightarrow 1^-0_n)$ $[e^2\ \text{fm}^2\times 10^{-3}]$ Expt.	Ref.	Calc. QPNM
^{156}Gd	2.5–3.3	9.5	[47]	10.5
^{158}Gd	2.8–3.9	11.2	[47]	10.1
^{160}Gd	2.0–3.2	10.2	[48]	7.7
^{162}Dy	2.5–3.0	9.0	[8]	10.0
^{164}Dy	2.0–4.0	30.0	[9]	36.0
^{166}Er	1.6–3.5	52.0	[33]	52.0
^{168}Er	1.7–4.0	52.0	[33]	52.0
^{172}Yb	2.0–3.7	49.1	[37]	34.0
^{174}Yb	3.0–3.7	23.0	[37]	19.5
^{178}Hf	2.0–4.0	12.7	[40]	12.0

$$\sum_n \Gamma_0^{\text{red}}(E1;0^+0_{\text{g.s.}}\rightarrow 1^-0_n)=10.1\ \text{meV/MeV}^3.$$

The $M1$ and $E1$ reduced widths are quite similar. In the experiments on ^{168}Er only three weaker $E1$ transitions with a tentative $K=1$ assignment have been detected.

For comparison of the intensities of the $M1$ and $E1$ transitions in even-even deformed nuclei, we computed the $M1$ and $E1$ reduced widths. The results of the calculations within the QPNM of the $M1$ and $E1$ with $\Delta K=0$ and $\Delta K=1$ widths summed in energy range 2–4 MeV are presented in Table VII. The computed summed $M1$ and $E1$ reduced widths are close to one another. It means that the intensity of the $E1$ and $M1$ transitions is quite similar in the energy range 2–4 MeV.

According to experimental data, the $B(E1;0^+0_{\text{g.s.}}\rightarrow 1^-0_n)$ values are larger than the $B(E1;0^+0_{\text{g.s.}}\rightarrow 1^-1_n)$ values in several even-even deformed nuclei. The summed $E1$ reduced widths with $\Delta K=0$ and $\Delta K=1$ are given in Table VII. As is shown in Table VII, the summed reduced widths for $E1$ transitions to the levels with $K^\pi=0^-$ is about three times as large as the levels with $K^\pi=1^-$. It is in agreement with the conclusion made in Ref. [24]. A situation is changing in ^{178}Hf where the $E1$, $\Delta K=0$ summed reduced width strongly decreases.

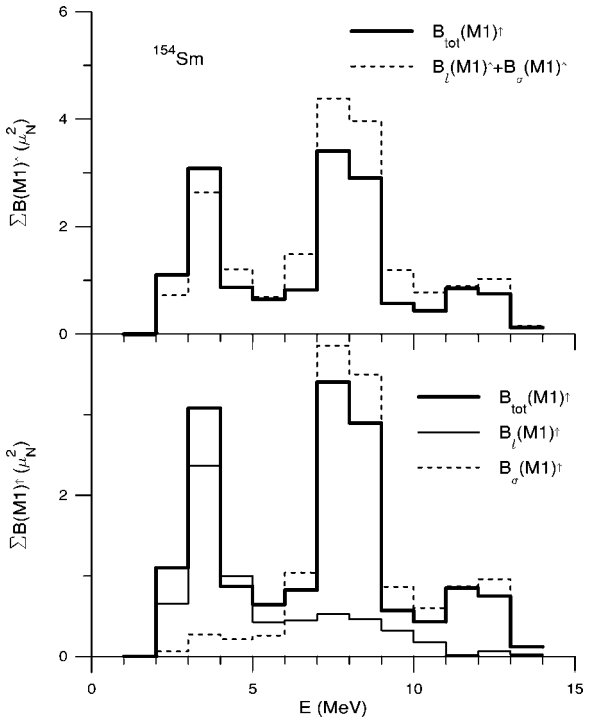

FIG. 8. RPA $M1$ strength distribution in ^{154}Sm in the 2–14 MeV energy range, summed in bins of 1 MeV. Total $\Sigma B_{\text{tot}}(M1)\uparrow$ and sum of orbital and spin $\Sigma B_l(M1)\uparrow+\Sigma B_\sigma(M1)\uparrow$ contributions (upper part) and total, orbital and spin contributions (lower part).

In conclusion, we can state the following.

(1) The $K^\pi=1^+$ states below 2 MeV in even-even nuclei are practically two-quasiparticle ones. Relevant experimental data are very scarce. For better understanding of a general situation with magnetic dipole excitations experimental measurement of the $M1$ and $E2$ transition rates for excitation of the $K^\pi=1^+$ states below 2 MeV is needed.

(2) The reduced transition widths $\Gamma_0^{\text{red}}(M1)$ and $\Gamma_0^{\text{red}}(E1)$ summed in the energy range 2–4 MeV are practically equal.

TABLE VII. Calculated in the QPNM $M1$ and $E1$ reduced widths, summed in the energy range 2–4 MeV.

Nucleus	$\Sigma_n\Gamma^{\text{red}}(M1;0^+0_{\text{g.s.}}\rightarrow 1^+1_n)$ meV/MeV^3	$\Sigma_n\Gamma^{\text{red}}(E1;0^+0_{\text{g.s.}}\rightarrow 1^-0_n)$ meV/MeV^3	$\Sigma_n\Gamma^{\text{red}}(E1;0^+0_{\text{g.s.}}\rightarrow 1^-1_n)$ meV/MeV^3
^{160}Gd	17.5	6.0	4.0
^{160}Dy	14.4	12.1	4.1
^{162}Dy	18.4	14.8	4.2
^{164}Dy	19.2	12.6	3.1
^{166}Er	12.8	13.3	3.6
^{168}Er	15.9	12.9	5.0
^{172}Yb	14.6	12.9	5.7
^{174}Yb	16.5	10.1	4.1
^{178}Hf	13.7	4.2	3.1

Therefore, it is necessary to measure the parity of the $K=1$ states.

(3) Fast $E1$ and $M1$ transitions are expected between large components of the wave functions differing by the octupole with $K=0$ or $K=1$ and quadrupole with $K=1$ phonon. It will be interesting to measure these fast γ-ray transition rates.

ACKNOWLEDGMENTS

We are grateful to P. von Neumann-Cosel and N. Pietralla for valuable discussions and for sending the experimental data before publication, and P. von Brentano, N. Lo Iudice, and R. D. Herzberg for useful discussions. This work was partly supported by Grant No. RFFR 96-15-96729.

[1] A. Richter, Nucl. Phys. **A507**, 99c (1990); **A522**, 139c (1991).
[2] U. Kneissl, H. H. Pitz, and A. Zilges, Prog. Part. Nucl. Phys. **37**, 349 (1996).
[3] N. Lo Iudice and F. Palumbo, Phys. Rev. Lett. **41**, 1532 (1978); G. De Franceschi, F. Palumbo, and N. Lo Iudice, Phys. Rev. C **29**, 1496 (1984).
[4] D. Bohle, A. Richter, W. Steffen, A. E. L. Dieperink, N. Lo Iudice, F. Palumbo, and O. Scholten, Phys. Lett. **137B**, 27 (1984).
[5] C. Djalali *et al.*, Phys. Lett. **164B**, 269 (1985).
[6] C. Wesselborg *et al.*, Z. Phys. A **323**, 485 (1986).
[7] D. Frekers *et al.*, Phys. Lett. B **218**, 439 (1989).
[8] H. Friedrichs *et al.*, Phys. Rev. C **45**, R892 (1992).
[9] J. Margraf *et al.*, Phys. Rev. C **52**, 2429 (1995).
[10] R. Nojarov and A. Faessler, Nucl. Phys. **A484**, 1 (1988).
[11] A. Faessler, R. Nojarov, and F. G. Scholz, Nucl. Phys. **A515**, 237 (1990).
[12] D. Zawischa, M. Macfalane, and J. Speth, Phys. Rev. C **42**, 1461 (1990).
[13] I. Hamamoto and C. Magnusson, Phys. Lett. B **312**, 267 (1992).
[14] P. Sarriguren, E. Moya de Guerra, R. Nojarov, and A. Faessler, J. Phys. G **19**, 291 (1993).
[15] A. A. Raduta, N. Lo Iudice, and I. I. Ursu, Nucl. Phys. **A584**, 84 (1995).
[16] V. G. Soloviev and A. V. Sushkov, Phys. Lett. B **262**, 189 (1991).
[17] V. G. Soloviev, Sov. J. Part. Nucl. **9**, 343 (1978).
[18] V. G. Soloviev, *Theory of Atomic Nuclei: Quasiparticles and Phonons* (Institute of Physics, Bristol and Philadelphia, 1992).
[19] V. G. Soloviev, A. V. Sushkov, N. Yu. Shirikova, and N. Lo Iudice, Nucl. Phys. **A600**, 155 (1996).
[20] V. G. Soloviev, A. V. Sushkov, and N. Yu. Shirikova, Phys. At. Nucl. **59**, 51 (1996).
[21] V. G. Soloviev, A. V. Sushkov, and N. Yu. Shirikova, Int. J. Mod. Phys. E **3**, 1227 (1994).
[22] V. G. Soloviev, A. V. Sushkov, and N. Yu. Shirikova, Phys. Part. Nuclei **27**, 667 (1996).
[23] V. G. Soloviev, A. V. Sushkov, and N. Yu. Shirikova, Z. Phys. A **358**, 287 (1997).
[24] V. G. Soloviev, A. V. Sushkov, and N. Yu. Shirikova, J. Phys. G **21**, 1217 (1995).
[25] V. G. Soloviev, A. V. Sushkov, and N. Yu. Shirikova, Phys. Part. Nuclei **25**, 377 (1994).
[26] G. J. Gallagher and S. A. Moszkowski, Phys. Rev. **111**, 1282 (1958).
[27] V. G. Soloviev, A. V. Sushkov, N. Yu. Shirikova, and N. Lo Iudice, Nucl. Phys. **A613**, 45 (1997).
[28] R. Nojarov, A. Faessler, and M. Dingfelder, Phys. Rev. C **51**, 2449 (1995).
[29] P. Sarriguren, E. Moya de Guerra, and R. Nojarov, Phys. Rev. C **54**, 690 (1996).
[30] D. Frekers *et al.*, Phys. Lett. B **244**, 179 (1990).
[31] V. G. Soloviev and A. V. Sushkov, Phys. At. Nucl. **57**, 1304 (1994).
[32] I. Hamamoto, Nucl. Phys. **A205**, 225 (1973); **A557**, 115c (1993).
[33] H. Maser *et al.*, Phys. Rev. C **53**, 2749 (1996).
[34] A. Faessler, R. Nojarov, and T. Taigel, Nucl. Phys. **A492**, 105 (1989).
[35] N. Lo Iudice and A. Richter, Phys. Lett. B **304**, 193 (1989).
[36] E. Browne, Nucl. Data Sheets **61**, 1 (1991).
[37] A. Zilges, P. von Brentano, C. Wesselborg, R. D. Heil, U. Kneissl, S. Lindenstruth, H. H. Pitz, U. Seeman, and R. Stock, Nucl. Phys. **A507**, 399 (1990).
[38] S. J. Freeman *et al.*, Phys. Lett. B **222**, 347 (1989).
[39] S. J. Freeman *et al.*, Nucl. Phys. **A552**, 10 (1993).
[40] N. Pietralla *et al.*, Nucl. Phys. **A618**, 141 (1997).
[41] C. Rangacharyulu, A. Richter, H. J. Wörtche, W. Ziegler, and R. F. Casten, Phys. Rev. C **43**, R949 (1991).
[42] V. G. Soloviev, Phys. Rev. C **51**, R2885 (1995).
[43] N. Pietralla, P. von Brentano, R. D. Hezberg, U. Kneissl, J. Margraf, H. Maser, H. H. Pitz, and A. Zilges, Phys. Rev. C **52**, R2317 (1995).
[44] R. D. Heil, H. H. Pitz, U. E. P. Berg, U. Kneissl, K. D. Hummel, G. Kilgus, D. Bohle, A. Richter, C. Wesselborg, and P. von Brentano, Nucl. Phys. **A476**, 39 (1988).
[45] P. von Neumann-Cosel, Prog. Part. Nucl. Phys. **38**, 213 (1997).
[46] V. G. Soloviev, A. V. Sushkov, and N. Yu. Shirikova, Phys. At. Nucl. **60**(10) (1997).
[47] H. H. Pitz, U. E. P. Berg, R. D. Heil, U. Kneissl, R. Stock, C. Wesselborg, and P. von Brentano, Nucl. Phys. **A492**, 411 (1989).
[48] H. Friedrichs *et al.*, Nucl. Phys. **A567**, 266 (1994).